

On Approximation in Deep Convolutional Networks: a Kernel Perspective

Alberto Bietti

alberto.bietti@nyu.edu*

December 23, 2024

Abstract

The success of deep convolutional networks on tasks involving high-dimensional data such as images or audio suggests that they are able to efficiently approximate certain classes of functions that are not cursed by dimensionality. In this paper, we study this theoretically and empirically through the lens of kernel methods, by considering multi-layer convolutional kernels, which have achieved good empirical performance on standard vision datasets, and provide theoretical descriptions of over-parameterized convolutional networks in certain regimes. We find that while expressive kernels operating on input patches are important at the first layer, simpler polynomial kernels can suffice in higher layers for good performance. For such simplified models, we provide a precise functional description of the RKHS and its regularization properties, highlighting the role of depth for capturing interactions between different parts of the input signal, and the role of pooling for encouraging smooth dependence on the global or relative positions of such parts.

1 Introduction

Deep convolutional models have been at the heart of the recent successes of deep learning in problems where the data consists of high-dimensional signals, such as image classification or speech recognition. The convolution and pooling operations in these architectures are known to be crucial for their practical success, yet our theoretical understanding of how they enable efficient learning is still limited.

One key difficulty for understanding such models is the curse of dimensionality: due to the high-dimensionality of the input data, it is hopeless to learn arbitrary functions from samples. For instance, classical non-parametric regression techniques for approximating Lipschitz or Sobolev functions typically require either low dimension or an order of smoothness of the target function comparable to the dimension in order to obtain good generalization (*e.g.*, Wainwright, 2019), which is a very strong assumption when dealing with high-dimensional signals. Thus, further assumptions on the target function are needed to make the problem more tractable, in a way that makes convolutions a useful modeling tool. Various works have studied approximation benefits with models that resemble deep convolutional architectures, for instance through hierarchical models with local connectivity (Mhaskar and Poggio, 2016; Schmidt-Hieber et al., 2020), or through structured tensor decompositions (Cohen and Shashua, 2017). Nevertheless, while such function classes may provide improved statistical efficiency, it is unclear if they can be learned with computationally efficient algorithms, which makes it difficult to assess the validity of these approximation models empirically.

In order to overcome the computational difficulties, we provide a different perspective based on kernel methods (*e.g.*, Schölkopf and Smola, 2001; Wahba, 1990), which are known to be computationally tractable with well-understood statistical and approximation properties. In particular, we consider “deep” structured kernels known as convolutional kernels, which have produced good empirical performance on standard

*Center for Data Science, New York University, New York.

computer vision benchmarks (Mairal et al., 2014; Mairal, 2016; Li et al., 2019; Shankar et al., 2020), and provide some theoretical understanding of learning with over-parameterized convolutional networks (CNNs) through tight connections with infinite-width networks (Daniely et al., 2016; Jacot et al., 2018; Arora et al., 2019; Bietti and Mairal, 2019b; Garriga-Alonso et al., 2019; Novak et al., 2019; Yang, 2019). While the fixed representations given by such kernels may not capture certain desired properties of deep learning, such as feature selection (Bach, 2017a; Chizat et al., 2019) or hierarchical learning (Allen-Zhu and Li, 2020; Chen et al., 2020), they may provide insight into the benefits of architectural choices. For fully-connected architectures, such kernels are rotation-invariant, and the corresponding functional spaces (RKHS) are well understood in terms of regularity properties on the sphere (*e.g.*, Smola et al., 2001; Bach, 2017a), but do not show any major differences between deep and shallow kernels (Bietti and Bach, 2021; Chen and Xu, 2021). In contrast, in this work we show that for convolutional kernels, the architecture and its depth plays an essential role for approximation.

Our main contribution is to study approximation properties of deep convolutional kernels by describing the functions in their RKHS, and by providing an explicit expression of their RKHS norm, which controls the regularization properties of the kernel, and hence its inductive bias. We focus on multi-layer kernels with patch extraction, non-linear kernel embeddings and linear pooling operations, following the construction of convolutional kernel networks (Mairal, 2016; Bietti and Mairal, 2019a), where the first layer consists of expressive dot-product kernels (such as Gaussian or arc-cosine kernels) applied to small-scale patches of the input signal, while subsequent layers use simpler polynomial kernels on the patches at larger scales. We show empirically on the Cifar10 dataset that such simplified architectures achieve comparable performance to models that use such expressive kernels at all layers. In contrast, the performance degrades significantly when using shallow (one-layer) convolutional kernels, or when making the first layer kernels on patches also polynomial. The use of polynomial kernels at higher layers then enables a precise study of the RKHS through kernel tensor products, with the RKHS consisting of additive models of interaction terms between different patches of the signal, as in functional ANOVA models (see, *e.g.*, Lin, 2000; Scetbon and Harchaoui, 2020; Wahba, 1990). We then show how the choices of pooling and patch sizes provide further regularization by encouraging similarity among the functions in different ways, such as by preventing the interaction functions to depend too strongly on the relative position of the different patches, or on their global position. We complement the paper with additional experiments using the same kernels as in our theory; among others, we find a simple two-layer kernel architecture that outperforms state-of-the-art convolutional kernels on Cifar10.

Related work. The study of kernels for neural networks date back to Neal (1996), and have more recently been used as theoretical models for deep learning (Cho and Saul, 2009; Daniely et al., 2016; Bach, 2017a; Lee et al., 2018; Matthews et al., 2018; Jacot et al., 2018). Convolutional kernels have been introduced both as effective modeling tools for vision tasks (Mairal et al., 2014; Mairal, 2016; Li et al., 2019; Shankar et al., 2020) and as models for infinite-width convolutional networks (Daniely et al., 2016; Garriga-Alonso et al., 2019; Novak et al., 2019; Bietti and Mairal, 2019b). Bietti and Mairal (2019a); Zhang et al. (2017) study approximation properties of convolutional kernels, showing that the RKHS contains certain convolutional networks with smooth activations, but do not precisely characterize the functional space or its regularization properties. Mhaskar and Poggio (2016); Poggio et al. (2017) discuss approximation benefits of deep network architectures with local connectivity, which resemble deep convolutional networks, however it is unclear if tractable algorithms exist for finding such networks. Cohen and Shashua (2016, 2017) study expressivity of certain convolutional architectures through the lens of hierarchical tensor decompositions; such tensor decompositions are shown to favor certain interactions between parts of the input versus others, in a way that is related to our work, however no algorithm is provided for learning such models, while we study precise approximation and regularization properties for (tractable) kernel methods. Scetbon and Harchaoui (2020) study statistical properties of ridge regression with a simple two-layer convolutional kernel with no pooling; the authors also rely on kernel tensor products, but do not highlight the role of the kernel architecture in determining approximation properties, in contrast to our work. Gunasekar et al. (2018) study regularization properties (also known as the “implicit bias”) of gradient descent on linear convolutional networks; our work may also be seen as studying implicit bias, but for infinite-width convolutional networks

with different architectures and non-linear activations in different training regimes known as “kernel” or “lazy” regimes (Chizat et al., 2019; Woodworth et al., 2020). Heckel and Soltanolkotabi (2020) study regularization properties of convolutional generator architectures in kernel regimes, where there is a single output signal/image and essentially no input; in contrast, we consider functions with scalar outputs and arbitrary signals as inputs, leading to regularization properties that consider variability both in terms of spatial location and signal values.

2 Learning Functions on Signals

In this section, we begin by introducing and motivating the problem of learning functions defined on signals such as images, which captures tasks such as image classification where deep convolutional networks are predominant. We then introduce the convolutional kernels we consider, and recall properties of dot-product kernels and kernel tensor products, which are key to our study of approximation.

2.1 Natural Signals and Curse of Dimensionality

We consider learning problems consisting of labeled examples $(x, y) \sim \rho$ from a data distribution ρ , where x is a discrete signal $x[u]$ with $u \in \Omega$ denoting the position (e.g., pixel location in an image) in a domain Ω , $x[u] \in \mathbb{R}^p$ (e.g., $p = 3$ for RGB pixels), and $y \in \mathbb{R}$ is a target label. In a non-parametric setup, statistical learning may be framed as trying to approximate the regression function

$$f^*(x) = \mathbb{E}_\rho[y|x]$$

using samples from the data distribution ρ . If f^* is only assumed to be Lipschitz, learning requires a number of samples that scales exponentially in the dimension (see, e.g., von Luxburg and Bousquet, 2004; Wainwright, 2019), a phenomenon known as the *curse of dimensionality*. In the case of natural signals, the dimension $d = p|\Omega|$ scales with the size of the domain $|\Omega|$ (e.g., the number of pixels), which is typically very large and thus makes this intractable. One common way to alleviate this is to assume that f^* is smooth, however the order of smoothness typically needs to be of the order of the dimension in order for the problem to become tractable, which is a very strong assumption here when d is very large. This highlights the need for more structured assumptions on f^* which may help overcome the curse of dimensionality.

Insufficiency of invariance and stability. Two geometric properties that have been successful for studying the benefits of convolutional architectures are (near-)translation invariance and stability to deformations. Various works have shown that certain convolutional models f yield good invariance and stability (Mallat, 2012; Bruna and Mallat, 2013; Bietti and Mairal, 2019a), in the sense that when \tilde{x} is a translation or a small deformation of x , then $|f(\tilde{x}) - f(x)|$ is small. Nevertheless, one can show that for band-limited signals (such as discrete signals), $\|\tilde{x} - x\|_2$ can be controlled in a similar way (though with worse constants, see Wiatowski and Bölcskei, 2018, Proposition 5), so that Lipschitz functions on such signals obey such stability properties. Thus, deformation stability is not a much stronger assumption than Lipschitzness, and is insufficient by itself to escape the curse of dimensionality.

Spatial localization. One successful strategy for learning image recognition models which predates deep learning is to rely on simple aggregations of local features. These may be extracted using hand-crafted procedures (Lowe, 1999; Sánchez et al., 2013; Jégou et al., 2011), or using learned feature extractors, either through learned filters in the early layers of a CNN (Zeiler and Fergus, 2014), or other procedures (e.g., Thiry et al., 2021). One simplified example that encodes such a prior is if the target function f^* only depends on the input image through a localized part of the input such as a patch $x_u = (x[u+v])_{v \in S} \in \mathbb{R}^{p|S|}$, where S is a small box centered around 0, that is, $f^*(x) = g^*(x_u)$. Then, if g^* is assumed to be Lipschitz, we would like a sample complexity that only scales exponentially in the dimension of a patch $p|S|$, which is much smaller

than dimension of the entire image $p|\Omega|$. This is indeed the case if we use a kernel defined on such patches, such as

$$K(x, x') = \sum_u k(x_u, x'_u),$$

where k is a “simple” kernel such as a dot-product kernel, as discussed in Appendix A. In contrast, if K is a dot-product kernel on the entire image, corresponding to an infinite-width limit of a fully-connected network, then approximation is more difficult and is generally cursed by the full dimension (see Appendix A). While some models of wide fully-connected networks provide some adaptivity to low-dimensional structures such as the variables in a patch (Bach, 2017a), no tractable algorithms are currently known to achieve such behavior provably, and it is reasonable to instead encode such prior information in a convolutional architecture.

Modeling interactions. Modeling interactions between elements of a system at different scales, possibly hierarchically, is important in physics and complex systems, in order to efficiently handle systems with large numbers of variables (Beylkin and Mohlenkamp, 2002; Hackbusch and Kühn, 2009). As an example, one may consider target functions $f^*(x)$ that consist of interaction functions of the form $g(x_p, x_q)$, where p, q denote locations of the corresponding patches, and higher-order interactions may also be considered. In the context of image recognition, while functions of a single patch may capture local texture information such as edges or color, such an interaction function may also respond to specific spatial configurations of relevant patches, which could perhaps help identify properties related to the “shape” of an object, for instance. If such functions g are too general, then the curse of dimensionality may kick in again when one considers more than a handful of patches. Certain idealized models of approximation may model such interactions more efficiently through hierarchical compositions (*e.g.*, Poggio et al., 2017) or tensor decompositions (Cohen and Shashua, 2016, 2017), though no tractable algorithms are known to find such models. In this work, we tackle this in a tractable way using multi-layer convolutional kernels. We show that they can model interactions through kernel tensor products, which define functional spaces that are typically much smaller and more structured than for a generic kernel on the full vector (x_p, x_q) .

2.2 Deep Convolutional Kernels

We now recall the construction of multi-layer convolutional kernels on discrete signals, following most closely the convolutional kernel network (CKN) architectures defined by Mairal (2016); Bietti and Mairal (2019a). We note that other kernels arising from infinite-width limits of convolutional neural networks, such as the conjugate (or NNGP) kernel, as well as the (convolutional) neural tangent kernel, take similar forms (Arora et al., 2019; Bietti and Mairal, 2019b; Garriga-Alonso et al., 2019; Novak et al., 2019; Yang, 2019). For simplicity, we will focus on discrete 1D input signals, though one may easily extend our results to 2D or higher-dimensional signals. We will assume periodic signals in order to avoid difficulties with border effects, or alternatively, a cyclic domain $\Omega = \mathbb{Z}/|\Omega|\mathbb{Z}$. A convolutional kernel of depth L may then be defined for input signals $x, x' \in L^2(\Omega, \mathbb{R}^p)$ by $K_L(x, x') = \langle \Psi(x), \Psi(x') \rangle$, through the explicit feature map

$$\Psi(x) = A_L M_L P_L \cdots A_1 M_1 P_1 x. \quad (1)$$

Here, P_ℓ, M_ℓ and A_ℓ are linear or non-linear operators corresponding to *patch extraction*, *kernel mapping* and *pooling*, respectively. They operate on *feature maps* in $L^2(\Omega_\ell)$ (with $\Omega_0 = \Omega$) with values in different Hilbert spaces, starting from $\mathcal{H}_0 := \mathbb{R}^p$, and are defined below. An illustration of this construction is given in Figure 1.

Patch extraction. Given a patch shape $S_\ell \subset \Omega_{\ell-1}$, such as $S_\ell = [-1, 0, 1]$ for one-dimensional patches of size 3, the operator P_ℓ is defined for $x \in L^2(\Omega_{\ell-1}, \mathcal{H}_{\ell-1})$ by

$$P_\ell x[u] = (x[u+v])_{v \in S_\ell} \in \mathcal{H}_{\ell-1}^{|S_\ell|}.$$

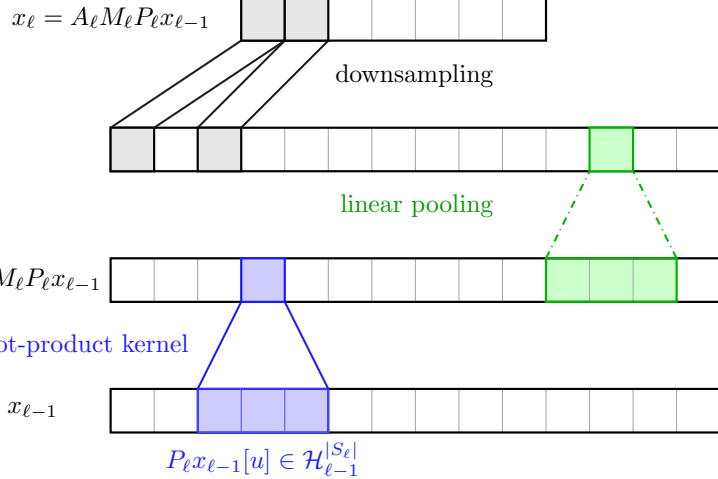


Figure 1: Illustration of the convolutional kernel construction.

Kernel mapping. The operators M_ℓ perform a non-linear embedding of patches into a new Hilbert space using dot-product kernels. We consider homogeneous dot-product kernels given for $z, z' \in \mathcal{H}_{\ell-1}^{|S_\ell|}$ by

$$k_\ell(z, z') = \|z\| \|z'\| \kappa_\ell \left(\frac{\langle z, z' \rangle}{\|z\| \|z'\|} \right) = \langle \varphi_\ell(z), \varphi_\ell(z') \rangle_{\mathcal{H}_\ell}, \quad (2)$$

where $\varphi_\ell : \mathcal{H}_{\ell-1}^{|S_\ell|} \rightarrow \mathcal{H}_\ell$ is a feature map for the kernel. The kernel functions take the form $\kappa_\ell(u) = \sum_{j \geq 0} b_j u^j$ with $b_j \geq 0$. This includes the exponential kernel $\kappa(u) = e^{\alpha(u-1)}$ (*i.e.*, Gaussian kernel on the sphere) and the arc-cosine kernel arising from random ReLU features (Cho and Saul, 2009), for which our construction is equivalent to that of the conjugate or NNGP kernel for an infinite-width random ReLU network with the same architecture. The operator M_ℓ is then defined pointwise by

$$M_\ell x[u] = \varphi_\ell(x[u]). \quad (3)$$

Pooling. Finally, the pooling operators A_ℓ perform local averaging through convolution with a filter $h_\ell[u]$, which we may consider to be symmetric ($h_\ell[-u] =: \bar{h}_\ell[u] = h_\ell[u]$). In practice, the pooling operation is often followed by downsampling by a factor s_ℓ , in which case the new signal $A_\ell x$ is defined on a new domain Ω_ℓ with $|\Omega_\ell| = |\Omega_{\ell-1}|/s_\ell$, and we may write for $x \in L^2(\Omega_{\ell-1})$ and $u \in \Omega_\ell$,

$$A_\ell x[u] = \sum_{v \in \Omega_{\ell-1}} h_\ell[s_\ell u - v] x[v]. \quad (4)$$

Our experiments consider Gaussian pooling filters with a size and bandwidth proportional to the downsampling factor s_ℓ , following Mairal (2016). In Section 3, we will often assume no downsampling for simplicity, in which case we may see the filter bandwidth as increasing with the layers.

2.3 Dot-Product Kernels and their Tensor Products

In this section, we review some properties of dot-product kernels, their induced RKHS and regularization properties. We then recall the notion of tensor product of kernels, which allows us to describe the RKHS of products of kernels in terms of that of individual kernels.

Dot-product kernels. The rotation-invariance of dot-product kernels provides a natural description of their RKHS in terms of harmonic decompositions of functions on the sphere using spherical harmonics (Smola et al., 2001; Bach, 2017a). This leads to natural connections with regularity properties of functions defined on the sphere. For instance, if the kernel integral operator on $L^2(\mathbb{S}^{d-1})$ has a polynomially decaying spectral decay, as is the case for kernels arising from the ReLU activation (Bach, 2017a; Bietti and Mairal, 2019b), then the RKHS contains functions $g \in L^2(\mathbb{S}^{d-1})$ with an RKHS norm equivalent to

$$\|\Delta_{\mathbb{S}^{d-1}}^{\beta/2} g\|_{L^2(\mathbb{S}^{d-1})}, \quad (5)$$

for some β that depends on the decay exponent and must be larger than $(d-1)/2$, with $\Delta_{\mathbb{S}^{d-1}}$ the Laplace-Beltrami operator on the sphere. This resembles a Sobolev norm of order β , and the RKHS contains functions with bounded derivatives up to order β . When d is small (e.g., at the first layer with small images patches), the space contains functions that need not be too regular, and may thus be quite discriminative, while for large d (e.g., for a fully-connected network), the functions must be highly smooth in order to be in the RKHS, and large norms are necessary to approach non-smooth functions. For kernels with decays faster than polynomial, such as the Gaussian kernel, the RKHS contains smooth functions, but may still provide good approximation to non-smooth functions, particularly with small d and when using small bandwidth parameters. The homogeneous case (2) leads to functions $f(x) = \|x\|g(\frac{x}{\|x\|})$ with g defined on the sphere, with a norm given by the same penalty (5) on the function g (Bietti and Mairal, 2019b).

Kernel tensor products. For more than one layer, the convolutional kernels we study in Section 3 can be expressed in terms of products of kernels on patches, of the form

$$K((x_1, \dots, x_m), (x'_1, \dots, x'_m)) = \prod_{j=1}^m k(x_j, x'_j), \quad (6)$$

where $x_1, \dots, x_m, x'_1, \dots, x'_m \in \mathbb{R}^d$ are patches which may come from different signal locations. If $\varphi : \mathbb{R}^d \rightarrow \mathcal{H}$ is the feature map into the RKHS \mathcal{H} of k , then

$$\psi(x_1, \dots, x_m) = \varphi(x_1) \otimes \dots \otimes \varphi(x_m)$$

is a feature map for K , and the corresponding RKHS, denoted $\mathcal{H}^{\otimes m} = \mathcal{H} \otimes \dots \otimes \mathcal{H}$, contains all functions

$$f(x_1, \dots, x_m) = \sum_{i=1}^n g_{i,1}(x_1) \dots g_{i,m}(x_m),$$

for some n , with $g_{i,m} \in \mathcal{H}$ for $i \in [n]$ and $j \in [m]$ (see, e.g., Wainwright, 2019, Section 12.4.2 for a precise construction). The resulting RKHS is often much smaller than for a more generic kernel on $\mathbb{R}^{d \times m}$; for instance, if \mathcal{H} is a Sobolev space of order β in dimension d , then $\mathcal{H}^{\otimes m}$ is much smaller than the Sobolev space of order β in $d \times m$ dimensions, and corresponds to stronger, mixed regularity conditions (see, e.g., Bach, 2017b; Sickel and Ullrich, 2009, for the $d=1$ case). This can yield improved generalization properties if the target function has such a structure (Lin, 2000). Kernels of the form (6) and sums of such kernels have been useful tools for avoiding the curse of dimensionality by encoding interactions between variables that are relevant to the problem at hand (Wahba, 1990, Chapter 10). In what follows, we show how patch extraction and pooling operations shape the properties of such interactions between patches in convolutional kernels through additional spatial regularities.

3 Approximation with (Deep) Convolutional Kernels

In this section, we present our main results on the approximation properties of convolutional kernels, by characterizing functions in the RKHS as well as their norms. We begin with the one-layer case, which does

not capture interactions between patches but highlights the role of pooling, before moving to the case of multiple layers where interaction terms play an important role. Unless otherwise specified, we consider invertible pooling operators A_ℓ with no downsampling ($s_\ell = 1$) for simplicity of presentation. Proofs are given in Appendix D.

3.1 The One-Layer Case

We begin by considering the case of a single convolutional layer, which can already help us illustrate the role of patches and pooling. Here, the kernel is given by

$$K_1(x, x') = \langle A\Phi(x), A\Phi(x') \rangle_{L^2(\Omega, \mathcal{H})},$$

with $\Phi(x)[u] = \varphi(x_u)$, where we use the shorthand $x_u = Px[u]$ for the patch at position u . We now characterize the RKHS of K_1 in terms of functions in \mathcal{H} defined on patches.

Proposition 1 (RKHS for 1-layer CKN.). *The RKHS of K_1 consists of functions $f(x) = \langle G, \Phi(x) \rangle = \sum_{u \in \Omega} G[u](x_u)$, with $G \in \text{Range}(A^\top)$, and with RKHS norm*

$$\begin{aligned} \|f\|_{\mathcal{H}_K}^2 &= \inf_{G \in L^2(\Omega, \mathcal{H})} \|A^{-\top} G\|_{L^2(\Omega, \mathcal{H})}^2 \\ \text{s.t. } &f(x) = \langle G, \Phi(x) \rangle. \end{aligned} \tag{7}$$

Note that if A^\top is not invertible (for instance in the presence of downsampling), then the inverse should be replaced by a pseudoinverse, and the constraint $G \in \text{Range}(A^\top)$ is active. In the extreme case of global average pooling, we have $A = (1, \dots, 1) \otimes \text{Id} : L^2(\Omega, \mathcal{H}) \rightarrow \mathcal{H}$, so that $G \in \text{Range}(A^\top)$ is equivalent to $G[u] = g$ for all u , for some fixed $g \in \mathcal{H}$. In this case, the penalty in (7) is simply the squared RKHS norm $\|g\|_{\mathcal{H}}^2$.

In order to understand the norm (7), note that A is a convolution operator, hence its inverse may be easily computed in the Fourier basis. In particular, for a patch $z \in \mathbb{R}^{p|S_1|}$, defining the scalar signal $g_z[u] = G[u](z)$, we may write the following using the reproducing property and linearity:

$$A^{-\top} G[u](z) = A^{-\top} g_z[u] = \mathcal{F}^{-1} \text{diag}(\mathcal{F} \bar{h}_1)^{-1} \mathcal{F} g_z[u],$$

where $\bar{h}_1[u] := h_1[-u]$, \mathcal{F} is the discrete Fourier transform, and both \mathcal{F} and A are viewed here as $|\Omega| \times |\Omega|$ matrices. From this expression, we see that by penalizing the RKHS norm of f , we are implicitly penalizing the high frequencies of the signals $g_z[u]$ for any z , and this regularization is stronger when the pooling filter h_1 has a fast spectral decay. For instance, as the spatial bandwidth of h_1 increases (approaching a global pooling operation), $\mathcal{F} h_1$ decreases more rapidly, which encourages $g_z[u]$ to be more smooth as a function of u , and thus prevents f from relying too much on the location of patches. If instead h_1 is very localized in space (e.g., a Dirac filter, which corresponds to no pooling), $g_z[u]$ may vary much more rapidly as a function of u , which then allows f to discriminate differently depending on the spatial location. This provides a different perspective on the invariance properties induced by pooling. If we denote $\tilde{G}[u] = A^{-\top} G[u]$, the penalty writes

$$\|\tilde{G}\|_{L^2(\Omega, \mathcal{H})}^2 = \sum_{u \in \Omega} \|\tilde{G}[u]\|_{\mathcal{H}}^2.$$

Here, the RKHS norm $\|\cdot\|_{\mathcal{H}}$ also controls smoothness, but this time for functions $\tilde{G}[u](\cdot)$ defined on input patches, typically through regularization operators on the sphere as described in Section 2.3. If for simplicity we assume that patches lie in the sphere \mathbb{S}^{d-1} , we may write $\|g\|_{\mathcal{H}} = \|T^{-1/2}g\|_{L^2(\mathbb{S}^{d-1})}$, where the regularization operator $T^{-1/2}$ is the self-adjoint square root of the integral operator for the patch kernel (2). Then we may write

$$\|\tilde{G}\|_{L^2(\Omega, \mathcal{H})}^2 = \|(A^{-\top} \otimes T^{-1/2})G\|_{L^2(\Omega) \otimes L^2(\mathbb{S}^{d-1})}^2,$$

which highlights that the norm applies two regularization operators A^{-1} and $T^{-1/2}$ independently on the spatial variable and the patch variable of $(u, z) \mapsto G[u](z)$, viewed here as an element of $L^2(\Omega) \otimes L^2(\mathbb{S}^{d-1})$.

Table 1: Cifar10 test accuracy with 2-layer convolutional kernels with 3x3 patches and pooling/downsampling sizes [2,5], with different choices of patch kernels κ_1 and κ_2 . The last model is similar to a 1-layer convolutional kernel. For computational reasons we only use the exact kernel on the full training set (50k images) for some of the models, but show results using 10k training images for all models. The numbers in parentheses are for the Nyström approximation approach of Mairal (2016) with [256,4096] filters, instead of the full kernel, which is computationally much cheaper. See Section 4 for experimental details.

κ_1	κ_2	Test acc. (10k)	Test acc. (full)
Exp	Exp	80.5%	87.9% (84.1%)
Exp	Poly3	80.5%	87.7% (84.1%)
Exp	Poly2	79.4%	86.9% (83.4%)
Poly2	Exp	77.4%	- (81.5%)
Poly2	Poly2	75.1%	- (81.2%)
Exp	- (Lin)	74.2%	- (76.3%)

3.2 The Multi-Layer Case

We now study the case of convolutional kernels with more than one convolutional layer. While the patch kernels used at higher layers are typically similar to the ones from the first layer, we show empirically on Cifar10 that they may be replaced by simple polynomial kernels with little loss in accuracy. We then proceed by studying the RKHS of such simplified models, highlighting the role of depth for capturing interactions between different patches via kernel tensor products.

An empirical study. Table 1 shows the performance of a given 2-layer convolutional kernel architecture, with different choices of patch kernels κ_1 and κ_2 . The reference model uses exponential kernels in both layers, following the construction of Mairal (2016). We find that replacing the second layer kernel by a simple polynomial kernel of degree 3, $\kappa_2(u) = u^3$, leads to roughly the same test accuracy. By changing κ_2 to $\kappa_2(u) = u^2$, the test accuracy is only about 1% lower, while doing the same for the first layer decreases it by at least 3%. The shallow kernel with a single non-linear convolutional layer (shown in the last line of Table 1) performs significantly worse, and even when using larger patches and different pooling sizes, we could not obtain more than 76% test accuracy on 10k training examples. Similar observations apply for the Nyström approximation of the kernel proposed by Mairal (2016), which is much more tractable computationally.¹ This suggests that the approximation properties described in Section 3.1 may not be sufficient for this task, while even a simple polynomial kernel of order 2 at the second layer may substantially improve things by capturing interactions, in a way that we describe below.

Two-layers with a quadratic kernel. Motivated by the above experiments, we now study the RKHS of a two-layer kernel $K_2(x, x') = \langle \Psi(x), \Psi(x') \rangle_{L^2(\Omega_2, \mathcal{H}_2)}$ with Φ as in (1) with $L = 2$, where the second-layer uses a quadratic kernel² on patches $k_2(z, z') = (z, z')^2$. An explicit feature map for k_2 is given by $\varphi_2(z) = z \otimes z$. Denoting by \mathcal{H} the RKHS of k_1 , the patches z lie in $\mathcal{H}^{|S_2|}$, thus we may view φ_2 as a feature map into a Hilbert space $\mathcal{H}_2 = (\mathcal{H} \otimes \mathcal{H})^{|S_2| \times |S_2|}$ (by isomorphism to $\mathcal{H}^{|S_2|} \otimes \mathcal{H}^{|S_2|}$). The following result characterizes the RKHS of such a 2-layer convolutional kernel. In it, we use the notations $\text{diag}(M)[u] = M[u, u]$ for $M \in L^2(\Omega^2)$, $\text{diag}(x)[u, v] = \mathbb{1}\{u=v\}x[u]$ for $x \in L^2(\Omega)$, and L_c denotes a translation operator $L_c x[u] = x[u - c]$.

Proposition 2 (RKHS of 2-layer CKN with quadratic k_2). *Let $\Phi(x) = (\varphi_1(x_u) \otimes \varphi_1(x_v))_{u, v \in \Omega} \in L^2(\Omega^2, \mathcal{H} \otimes$*

¹We note that using more filters may increase accuracy to about 86% for the top model, see <https://gitlab.inria.fr/mairal/ckn-cudnn-matlab>.

²For simplicity we study the quadratic kernel instead of the homogeneous version used in the experiments, but we note that it still performs well (78.0% instead of 79.4% on 10k examples).



Figure 2: Visualization of the response of the operator E_{pq} to Dirac inputs $x = \delta_u$ centered at two different locations u . These are bumps centered on points of the $p - q$ diagonal, corresponding to interactions between two patches, at distance around $p - q$.

$\mathcal{H})$ The RKHS of K_2 when $k_2(z, z') = (\langle z, z' \rangle)^2$ consists of functions of the form

$$f(x) = \sum_{p, q \in S_2} \langle G_{pq}, \Phi(x) \rangle = \sum_{p, q \in S_2} \sum_{u, v \in \Omega} G_{pq}[u, v](x_u, x_v),$$

where $G_{pq} \in L^2(\Omega^2, \mathcal{H} \otimes \mathcal{H})$ obeys the constraints $G_{pq} \in \text{Range}(E_{pq})$, where the linear operator $E_{pq} : L^2(\Omega_1) \rightarrow L^2(\Omega^2)$ is given by

$$E_{pq}x = (L_p A_1 \otimes L_q A_1)^\top \text{diag}(x),$$

and $\text{diag}((L_p A_1 \otimes L_q A_1)^\top G_{pq}) \in \text{Range}(A_2^\top)$.

The squared RKHS norm $\|f\|_{\mathcal{H}_{K_2}}^2$ is then equal to the minimum over such decompositions of the quantity

$$\sum_{p, q \in S_2} \|A_2^{-\top} \text{diag}((L_p A_1 \otimes L_q A_1)^\top G_{pq})\|_{L^2(\Omega_2, \mathcal{H} \otimes \mathcal{H})}^2.$$

As discussed in the one-layer case, the inverses should be replaced by pseudo-inverses if needed, *e.g.*, when using downsampling. In particular, if A_2^\top is singular, the second constraint plays a similar role to the one-layer case. In order to understand the first constraint, we show in Figure 2 the outputs of $E_{pq}x$ for Dirac delta signals $x[v] = \delta_u[v]$. We can see that if the pooling filter h_1 has a small support of size m , then $G_{pq}[u - p, v - q]$ must be zero when $|u - v| > m$, which highlights that the functions in G_{pq} may only capture interactions between pairs of patches where the (signed) distance between the first and the second is close to $p - q$.

The penalty then involves operators $L_p A_1 \otimes L_q A_1$, which may be seen as separable 2D convolutions on the “images” $G_{pq}[u, v]$. Then, if $z, z' \in \mathbb{R}^{p|S_1|}$ are two fixed patches, defining $g_{z, z'}[u, v] = G_{pq}[u, v](z, z')$, we have

$$\begin{aligned} & (L_p A_1 \otimes L_q A_1)^\top G_{pq}[u, v](z, z') \\ &= (A_1 \otimes A_1)^\top g_{z, z'}[u - p, v - q] \\ &= \mathcal{F}_2^{-1} \text{diag}(\mathcal{F}_2(h_1 \otimes h_1))^{-1} \mathcal{F}_2 g_{z, z'}[u - p, v - q], \end{aligned}$$

where $\mathcal{F}_2 = \mathcal{F} \otimes \mathcal{F}$ is the 2D discrete Fourier transform. Thus, this penalizes the variations of $g_{z, z'}$ in both dimensions, encouraging the interaction functions to not rely too strongly on the specific positions of the two patches. The imposed smoothness will be larger when the spatial bandwidth of h_1 is larger, since the filter is then more localized in the frequency domain and hence induces stronger penalties for high frequencies. In addition to this 2D smoothness, the penalty in Proposition 2 also encourages smoothness along the $p - q$ diagonal of this resulting smoothed 2D image using the pooling operator A_2 . This has a similar behavior to the one-layer case, where the penalty prevents the functions from relying too much on the absolute position of the patches. Since A_2 typically has a larger bandwidth than A_1 , interaction functions $G_{pq}[u, u + r]$ are

allowed to vary with r more rapidly than with u . The regularity of the resulting “smoothed” interaction terms as a function of the input patches is controlled by the RKHS norm of the tensor product kernel $k_1 \otimes k_1$ as described in Section 2.3.

Extensions. When using a polynomial kernel $k_2(z, z') = (\langle z, z' \rangle)^\alpha$ with $\alpha > 2$, we obtain a similar picture as above, with higher-order interaction terms. For example, if $\alpha = 3$, the RKHS contains functions with interaction terms of the form $G_{pqr}[u, v, w](x_u, x_v, x_w)$, with a penalty

$$\sum_{p, q, r \in S_2} \|A_2^{-\top} \text{diag}((A_{1p} \otimes A_{1q} \otimes A_{1r})^{-\top} G_{pqr})\|_{L^2(\Omega_2, \mathcal{H}^{\otimes 3})}^2,$$

where $A_{1c} = L_c A_1$. Similarly to the quadratic case, the first-layer pooling operator encourages smoothness with respect to relative positions between patches, while the second-layer pooling penalizes dependence on the global location. One may extend this further to higher orders to capture more complex interactions, and our experiments suggest that a two-layer kernel of this form with a degree-4 polynomial at the second layer may achieve state-of-the-art accuracy for kernel methods on Cifar10 (see Table 3). We note that such fixed-order choices for κ_2 lead to convolutional kernels that lower-bound richer kernels with, *e.g.*, an exponential kernel at the second layer, in the Loewner order on positive-definite kernels. This implies in particular that the RKHS of these “richer” kernels also contains the functions described above. For more than two layers with polynomial kernels, one similarly obtains higher-order interactions, but with different regularization properties (see Appendix C).

4 Numerical Experiments

In this section, we provide additional experiments illustrating numerical properties of the convolutional kernels considered in this paper. We focus here on the Cifar10 dataset, and on convolutional kernels based on the exponential kernel on patches. Additional results with different architectures and datasets are given in Appendix B.

Experimental setup on Cifar10. We consider classification on Cifar10 dataset, which consists of 50k training images and 10k test images with 10 different output categories. We pre-process the images using a whitening/ZCA step at the patch level, which is commonly used for such kernels on images (Mairal, 2016; Shankar et al., 2020; Thiry et al., 2021). This may help reduce the effective dimensionality of patches, and better align the dominant eigen directions to the target function, a property which may help kernel methods (Ghorbani et al., 2020). Our convolutional kernel evaluation code is written in C++ and leverages the Eigen library for hardware-accelerated numerical computations. The computation of kernel matrices is distributed on up to 1000 cores on a cluster consisting of Intel Xeon processors. Computing the full Cifar10 kernel matrix typically takes around 10 hours when running on all 1000 cores. Due to the large computational cost, we only use the full dataset for a few selected models, and limit computations to 10k examples otherwise, noting that we have found the ordering between different models to usually remain stable across different sample sizes. Our results use kernel ridge regression in a one-versus-all approach, where each class uses labels 0.9 for the correct label and -0.1 for the other labels. When using the full Cifar10 dataset, we report the test accuracy for a fixed regularization parameter $\lambda = 10^{-8}$ (we note that the performance typically remains the same for smaller values of λ). For the results on 10k examples, we allow ourselves to optimize λ over a grid of values in $\{10^{-j}\}_{j=4, \dots, 10}$, in order to focus our attention on approximation properties rather than model selection. The exponential kernel always refers to $\kappa(u) = e^{\frac{1}{\sigma^2}(u-1)}$ with $\sigma = 0.6$. Our code is available at https://github.com/albietz/ckn_kernel.

Varying the kernel architecture. Table 2 shows test accuracies for 3-layer convolutional kernels with patch size 3x3 and pooling with downsampling factor 2 at each layer. The full model with exponential kernels outperforms the 2-layer architecture of Table 1, and the accuracy on the full dataset matches the

Table 2: Cifar10 test accuracy with 3-layer convolutional kernels with 3×3 patches and pooling/downsampling sizes $[2,2,2]$, with different choices of patch kernels κ_1 , κ_2 and κ_3 . The last model is similar to a 1-layer convolutional kernel. For computational reasons we use 10k training images instead of the full training set (50k images) in most cases.

κ_1	κ_2	κ_3	Test ac. (10k)	Test ac. (50k)
Exp	Exp	Exp	80.7%	88.2%
Exp	Poly2	Poly2	80.5%	87.9%
Exp	Poly4	Lin	80.2%	-
Exp	Lin	Poly4	79.2%	-
Exp	Lin	Lin	74.1%	-

Table 3: Cifar10 test accuracy with 2-layer convolutional kernels with 3×3 patches at the first layer and pooling/downsampling sizes $[2,5]$, with different choices of patch kernels κ_1/κ_2 and different patch sizes at the second layer.

κ_1	κ_2	$ S_2 $	Test ac. (10k)	Test ac. (50k)
Exp	Exp	5x5	81.1%	88.3%
Exp	Poly4	5x5	81.3%	88.3%
Exp	Poly3	5x5	81.1%	-
Exp	Poly2	7x7	80.1%	-
Exp	Poly2	5x5	80.1%	-
Exp	Poly2	3x3	79.4%	-
Exp	Poly2	1x1	76.3%	-

state-of-the-art kernels of (Shankar et al., 2020), which use a more complex 10-layer architecture.³ We also find see that using degree-2 polynomial kernels at the second and third layer only results in a 0.2% accuracy drop. This structure, which captures interactions of order 4, also outperforms the simpler ones using degree-4 kernels at either layer, suggesting that a deeper architecture may better model relevant interactions terms on this problem.

In Table 3, we illustrate the performance of two-layer models with different architectures than the one considered in Table 1. In particular, we find that using bigger patches at the second layer can in fact lead to better performance even than the three-layer model presented above, leading to a **state-of-the-art** accuracy for kernels on Cifar10 of 88.3%. Replacing the exponential kernel at the second layer by polynomial kernels of degree 3 or 4 preserves essentially the same accuracy, while a degree-2 polynomials loses about 1%, suggesting that certain Cifar10 images may require capturing interactions between at least 3 different patches in the image for good classification. While these results are encouraging, computing such kernels is prohibitively costly, and we found that applying the Nyström approach of Mairal (2016) to this kernel with larger patches requires larger models than for the architecture of Table 1 for a similar accuracy.

Role of pooling. Figure 3 shows the spectral decays of the empirical kernel matrix on 1000 Cifar images, which may help assess the “effective dimensionality” of the data, and are related to generalization properties (Caponnetto and De Vito, 2007). While multi-layer architectures with pooling seem to provide comparable comparable decays for various depths, removing pooling leads to significantly slower decays, and hence much larger RKHSs. In particular, the “strided pooling” architecture (*i.e.*, with Dirac pooling filters and downsampling) shown in Figure 3(right), which resembles the kernel considered by Scetbon and Harchaoui (2020), obtains less than 40% accuracy on 10k examples. This suggests that the regularization properties induced by pooling, studied in Section 3, are crucial for efficient approximation on these problems.

³We refer here to the Myrtle10-Gaussian Kernel model of Shankar et al. (2020), which achieves 88.2% accuracy without data augmentation.

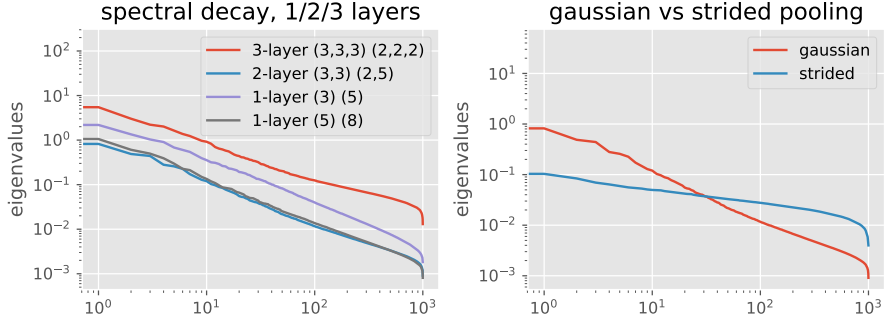


Figure 3: Eigenvalue decays of kernel matrices (with Exp kernels) on 1000 Cifar images. (left) different depths, patch sizes (3 or 5) and pooling sizes. (right) 2-layer architecture, Gaussian pooling filter vs strided pooling.

5 Discussion and Concluding Remarks

In this paper, we studied approximation properties of convolutional kernels, showing how multi-layer models with convolutional architectures may effectively break the curse of dimensionality on problems where the input consists of high-dimensional natural signals, by modeling localized functions on patches and interactions thereof. We also show how pooling induces additional smoothness constraints on how interaction terms may or may not vary with global and relative spatial locations. A natural question for future work is to study statistical properties of learning with such kernels through a precise study of eigenvalue decays of the covariance operator. Another important question is how optimization of deep convolutional networks may further improve approximation properties compared to what is captured by the kernel regime presented here, in particular how depth may play a more prominent role perhaps through hierarchy (*e.g.*, Allen-Zhu and Li, 2020; Chen et al., 2020).

Acknowledgements

The author thanks Francis Bach, Alessandro Rudi, and Joan Bruna for helpful discussions, and Julien Mairal for providing access to the Inria Thoth computing cluster.

References

- Z. Allen-Zhu and Y. Li. Backward feature correction: How deep learning performs deep learning. *arXiv preprint arXiv:2001.04413*, 2020.
- S. Arora, S. S. Du, W. Hu, Z. Li, R. R. Salakhutdinov, and R. Wang. On exact computation with an infinitely wide neural net. In *Advances in Neural Information Processing Systems (NeurIPS)*, 2019.
- F. Bach. Breaking the curse of dimensionality with convex neural networks. *Journal of Machine Learning Research (JMLR)*, 18(1):629–681, 2017a.
- F. Bach. On the equivalence between kernel quadrature rules and random feature expansions. *Journal of Machine Learning Research (JMLR)*, 18(1):714–751, 2017b.
- G. Beylkin and M. J. Mohlenkamp. Numerical operator calculus in higher dimensions. *Proceedings of the National Academy of Sciences*, 99(16):10246–10251, 2002.
- A. Bietti and F. Bach. Deep equals shallow for ReLU networks in kernel regimes. In *Proceedings of the International Conference on Learning Representations (ICLR)*, 2021.

A. Bietti and J. Mairal. Group invariance, stability to deformations, and complexity of deep convolutional representations. *Journal of Machine Learning Research (JMLR)*, 20(25):1–49, 2019a.

A. Bietti and J. Mairal. On the inductive bias of neural tangent kernels. In *Advances in Neural Information Processing Systems (NeurIPS)*, 2019b.

J. Bruna and S. Mallat. Invariant scattering convolution networks. *IEEE Transactions on Pattern Analysis and Machine Intelligence (PAMI)*, 35(8):1872–1886, 2013.

A. Caponnetto and E. De Vito. Optimal rates for the regularized least-squares algorithm. *Foundations of Computational Mathematics*, 7(3):331–368, 2007.

L. Chen and S. Xu. Deep neural tangent kernel and laplace kernel have the same rkhs. In *Proceedings of the International Conference on Learning Representations (ICLR)*, 2021.

M. Chen, Y. Bai, J. D. Lee, T. Zhao, H. Wang, C. Xiong, and R. Socher. Towards understanding hierarchical learning: Benefits of neural representations. In *Advances in Neural Information Processing Systems (NeurIPS)*, 2020.

L. Chizat, E. Oyallon, and F. Bach. On lazy training in differentiable programming. In *Advances in Neural Information Processing Systems (NeurIPS)*, 2019.

Y. Cho and L. K. Saul. Kernel methods for deep learning. In *Advances in Neural Information Processing Systems (NIPS)*, 2009.

C. Ciliberto, F. Bach, and A. Rudi. Localized structured prediction. In *Advances in Neural Information Processing Systems (NeurIPS)*, 2019.

N. Cohen and A. Shashua. Convolutional rectifier networks as generalized tensor decompositions. In *Proceedings of the International Conference on Machine Learning (ICML)*, 2016.

N. Cohen and A. Shashua. Inductive bias of deep convolutional networks through pooling geometry. In *Proceedings of the International Conference on Learning Representations (ICLR)*, 2017.

A. Daniely, R. Frostig, and Y. Singer. Toward deeper understanding of neural networks: The power of initialization and a dual view on expressivity. In *Advances in Neural Information Processing Systems (NIPS)*, 2016.

A. Garriga-Alonso, L. Aitchison, and C. E. Rasmussen. Deep convolutional networks as shallow gaussian processes. In *Proceedings of the International Conference on Learning Representations (ICLR)*, 2019.

B. Ghorbani, S. Mei, T. Misiakiewicz, and A. Montanari. When do neural networks outperform kernel methods? In *Advances in Neural Information Processing Systems (NeurIPS)*, 2020.

S. Gunasekar, J. D. Lee, D. Soudry, and N. Srebro. Implicit bias of gradient descent on linear convolutional networks. In *Advances in Neural Information Processing Systems (NeurIPS)*, 2018.

W. Hackbusch and S. Kühn. A new scheme for the tensor representation. *Journal of Fourier analysis and applications*, 15(5):706–722, 2009.

K. He, X. Zhang, S. Ren, and J. Sun. Deep residual learning for image recognition. In *Proceedings of the IEEE Conference on Computer Vision and Pattern Recognition (CVPR)*, 2016.

R. Heckel and M. Soltanolkotabi. Denoising and regularization via exploiting the structural bias of convolutional generators. In *Proceedings of the International Conference on Learning Representations (ICLR)*, 2020.

A. Jacot, F. Gabriel, and C. Hongler. Neural tangent kernel: Convergence and generalization in neural networks. In *Advances in Neural Information Processing Systems (NIPS)*, 2018.

H. Jégou, F. Perronnin, M. Douze, J. Sánchez, P. Pérez, and C. Schmid. Aggregating local image descriptors into compact codes. *IEEE Transactions on Pattern Analysis and Machine Intelligence (PAMI)*, 34(9):1704–1716, 2011.

J. Lee, Y. Bahri, R. Novak, S. S. Schoenholz, J. Pennington, and J. Sohl-Dickstein. Deep neural networks as gaussian processes. In *Proceedings of the International Conference on Learning Representations (ICLR)*, 2018.

Z. Li, R. Wang, D. Yu, S. S. Du, W. Hu, R. Salakhutdinov, and S. Arora. Enhanced convolutional neural tangent kernels. *arXiv preprint arXiv:1911.00809*, 2019.

Y. Lin. Tensor product space anova models. *Annals of Statistics*, 28(3):734–755, 2000.

D. G. Lowe. Object recognition from local scale-invariant features. In *Proceedings of the IEEE Conference on Computer Vision and Pattern Recognition (CVPR)*, 1999.

J. Mairal. End-to-End Kernel Learning with Supervised Convolutional Kernel Networks. In *Advances in Neural Information Processing Systems (NIPS)*, 2016.

J. Mairal, P. Koniusz, Z. Harchaoui, and C. Schmid. Convolutional kernel networks. In *Advances in Neural Information Processing Systems (NIPS)*, 2014.

E. Malach and S. Shalev-Shwartz. Computational separation between convolutional and fully-connected networks. In *Proceedings of the International Conference on Learning Representations (ICLR)*, 2021.

S. Mallat. Group invariant scattering. *Communications on Pure and Applied Mathematics*, 65(10):1331–1398, 2012.

A. Matthews, M. Rowland, J. Hron, R. E. Turner, and Z. Ghahramani. Gaussian process behaviour in wide deep neural networks. *arXiv preprint arXiv:1804.11271*, 2018.

H. N. Mhaskar and T. Poggio. Deep vs. shallow networks: An approximation theory perspective. *Analysis and Applications*, 14(06):829–848, 2016.

R. M. Neal. *Bayesian learning for neural networks*. Springer, 1996.

R. Novak, L. Xiao, Y. Bahri, J. Lee, G. Yang, J. Hron, D. A. Abolafia, J. Pennington, and J. Sohl-Dickstein. Bayesian deep convolutional networks with many channels are gaussian processes. In *Proceedings of the International Conference on Learning Representations (ICLR)*, 2019.

T. Poggio, H. Mhaskar, L. Rosasco, B. Miranda, and Q. Liao. Why and when can deep-but not shallow- networks avoid the curse of dimensionality: a review. *International Journal of Automation and Computing*, 14(5):503–519, 2017.

S. Saitoh. *Integral transforms, reproducing kernels and their applications*, volume 369. CRC Press, 1997.

J. Sánchez, F. Perronnin, T. Mensink, and J. Verbeek. Image classification with the fisher vector: Theory and practice. *International Journal of Computer Vision (IJCV)*, 105(3):222–245, 2013.

M. Scetbon and Z. Harchaoui. Harmonic decompositions of convolutional networks. In *Proceedings of the International Conference on Machine Learning (ICML)*, 2020.

J. Schmidt-Hieber et al. Nonparametric regression using deep neural networks with relu activation function. *Annals of Statistics*, 48(4):1875–1897, 2020.

B. Schölkopf and A. J. Smola. *Learning with kernels: support vector machines, regularization, optimization, and beyond*. 2001.

V. Shankar, A. Fang, W. Guo, S. Fridovich-Keil, J. Ragan-Kelley, L. Schmidt, and B. Recht. Neural kernels without tangents. In *Proceedings of the International Conference on Machine Learning (ICML)*, 2020.

W. Sickel and T. Ullrich. Tensor products of sobolev–besov spaces and applications to approximation from the hyperbolic cross. *Journal of Approximation Theory*, 161(2):748–786, 2009.

A. J. Smola, Z. L. Ovari, and R. C. Williamson. Regularization with dot-product kernels. In *Advances in Neural Information Processing Systems (NIPS)*, 2001.

L. Thiry, M. Arbel, E. Belilovsky, and E. Oyallon. The unreasonable effectiveness of patches in deep convolutional kernels methods. In *Proceedings of the International Conference on Learning Representations (ICLR)*, 2021.

U. von Luxburg and O. Bousquet. Distance-based classification with lipschitz functions. *Journal of Machine Learning Research (JMLR)*, 5(Jun):669–695, 2004.

G. Wahba. *Spline models for observational data*, volume 59. Siam, 1990.

M. J. Wainwright. *High-dimensional statistics: A non-asymptotic viewpoint*, volume 48. Cambridge University Press, 2019.

T. Wiatowski and H. Bölcsei. A mathematical theory of deep convolutional neural networks for feature extraction. *IEEE Transactions on Information Theory*, 64(3):1845–1866, 2018.

B. Woodworth, S. Gunasekar, J. D. Lee, E. Moroshko, P. Savarese, I. Golan, D. Soudry, and N. Srebro. Kernel and rich regimes in overparametrized models. In *Conference on Learning Theory (COLT)*, 2020.

G. Yang. Scaling limits of wide neural networks with weight sharing: Gaussian process behavior, gradient independence, and neural tangent kernel derivation. *arXiv preprint arXiv:1902.04760*, 2019.

M. D. Zeiler and R. Fergus. Visualizing and understanding convolutional networks. In *Proceedings of the European Conference on Computer Vision (ECCV)*, 2014.

Y. Zhang, P. Liang, and M. J. Wainwright. Convexified convolutional neural networks. In *International Conference on Machine Learning (ICML)*, 2017.

A Complexity of Spatially Localized Functions

In this section, we briefly elaborate on our discussion in Section 2.1 on how simple convolutional structure may improve complexity when target functions are spatially localized. We assume $f^*(x) = g^*(x_u)$ with $x_u = [x|u+v]_{v \in S} \in \mathbb{R}^{p|S|}$ a patch of size $|S|$, where g^* is a Lipschitz function.

If we define the kernel $K_u(x, x') = k(x_u, x'_u)$, where k is a dot-product kernel arising from a one-hidden layer network with positively-homogeneous activation such as the ReLU, and further assume patches to be bounded and g^* to be bounded, then the uniform approximation error bound of Bach (2017a, Proposition 6) together with a simple $O(1/\sqrt{n})$ Rademacher complexity bound on estimation error shows that we may achieve a generalization bound with a rate that only depends on the patch dimension $p|S|$ rather than $p|\Omega|$ in this setup (*i.e.*, a sample complexity that is exponential in $p|S|$, which is much smaller than $p|\Omega|$).

If we consider the kernel $K(x, x') = \sum_{u \in \Omega} k(x_u, x'_u)$, the RKHS contains all functions in the RKHS of K_u for all $u \in \Omega$, with the same norm (this may be seen as an application of Theorem 4 with a feature map given by concatenating the kernel maps of each K_u), so that we may achieve the same approximation error as above, and thus a similar generalization bound that is not cursed by dimension. This kernel also allows us to obtain similar generalization guarantees when f^* consists of linear combinations of such spatially localized functions on different patches within the image.

In contrast, when using a similar dot-product kernel on the full signal, corresponding to using a fully-connected network in a kernel regime, one may construct functions $f^*(x) = g^*(x_u)$ with g^* Lipschitz where an RKHS norm that is exponentially large in the (full) dimension $p|\Omega|$ is needed for a small approximation error (see Bach, 2017a, Appendix D.5).

Related to this, Malach and Shalev-Shwartz (2021) show a separation in the different setting of learning certain parity functions on the hypercube using gradient methods; their upper bound for convolutional networks is based on a similar kernel regime as above. We note that kernels that exploit such a localized structure have also been considered in the context of structured prediction for improved statistical guarantees (Ciliberto et al., 2019).

B Additional experiments

In this section, we provide additional experiments to those presented in Section 4, using different patch kernels, larger patches, and a different dataset.

Table 4: Cifar10 test accuracy with patch kernels that are either arc-cosine kernels (denoted ReLU) or polynomial kernels. The 2-layer architectures use 3x3 patches and [2,5] downsampling/pooling as in Table 1. “ReLU-NTK” indicates that we consider the neural tangent kernel for a ReLU network with similar architecture, instead of the conjugate kernel.

κ_1	κ_2	Test ac. (10k)	Test ac. (50k)
ReLU	ReLU	78.5%	86.6%
ReLU-NTK	ReLU-NTK	79.2%	87.2%
ReLU	Poly2	77.2%	-
ReLU	Lin	71.5%	-

Arc-cosine kernel. In Table 4, we consider 2-layer convolutional kernels with a similar architecture to those considered in Table 1, but where we use arc-cosine kernels arising from ReLU activations instead of the exponential kernel used in Section 4, given by

$$\kappa(u) = \frac{1}{\pi}(u \cdot (\pi - \arccos(u)) + \sqrt{1 - u^2}).$$

The obtained convolutional kernel then corresponds to the conjugate kernel or NNGP kernel arising from an infinite-width convolutional network with the ReLU activation (Daniely et al., 2016; Garriga-Alonso et al.,

2019; Novak et al., 2019). We may also consider the neural tangent kernel (NTK) for the same architecture, which additionally involves arc-cosine kernels of degree 0, which correspond to random feature kernels for step activations $u \mapsto \mathbb{1}\{u \geq 0\}$. We find that the NTK performs slightly better than the conjugate kernel, but both kernels achieve lower accuracy compared to the Exponential kernel shown in Table 1. Nevertheless, we observe a similar pattern regarding the use of polynomial kernels at the second layer, namely, the drop in accuracy is much smaller when using a quadratic kernel compared to a linear kernel, suggesting that non-linear kernels on top of the first layer, and the interactions they may capture, are crucial on this dataset for good accuracy.

Table 5: Cifar10 test accuracy for one-layer architectures with larger patches of size 6x6, exponential kernels, and different downsampling/pooling sizes (using Gaussian pooling filters with bandwidth and size of filters proportional to the downsampling factor). The results are for 10k training samples.

Pooling	2	4	6	8	10
Test acc. (10k)	67.6%	73.3%	75.5%	75.8%	75.5%

One-layer architectures and larger initial patches. Table 5 shows the accuracy for one-layer convolutional kernels with 6x6 patches⁴ and various pooling sizes, with a highest accuracy of 75.8% for a pooling size of 8. While this improves on the accuracy obtained with 3x3 patches (slightly above 74% for the architectures in Tables 1 and 2 with a single non-linear kernel at the first layer), these accuracies remain much lower than those achieved by two-layer architectures with even quadratic kernels at the second layer. While using larger patches may allow capturing patterns that are less localized compared to small 3x3 patches, the neighborhoods that they model need to remain small in order to avoid the curse of dimensionality when using dot-product kernels, as discussed in Section 2. Instead, the multi-layer architecture may model information at larger scales with a much milder dependence on the size of the neighborhood, thanks to the structure imposed by tensor product kernels (see Section 2.3) and the additional regularities induced by pooling.

We also found that larger patches at the first layer may hurt performance in multi-layer models: when considering the architecture of Table 1 with exponential kernels, using 5x5 patches instead of 3x3 at the first layer yields an accuracy of 79.6% instead of 80.5% on Cifar10 when training on the same 10k images. This again reflects the benefits of using small patches at the first layer for allowing better approximation on small neighborhoods, while modeling larger scales using interaction models according to the structure of the architecture. We note nevertheless that for standard deep networks, larger patches are often used at the first layer (*e.g.*, He et al., 2016), as the feature selection capabilities of SGD may alleviate the dependence on dimension, *e.g.*, by finding Gabor-like filters.

Table 6: SVHN test accuracy for a two-layer convolutional kernel network with Nyström approximation (Mairal, 2016) with patch size 3x3, pooling sizes [2,5], and filters [256, 4096].

κ_1	κ_2	Test acc. (full with Nyström)
Exp	Exp	89.5%
Exp	Poly3	89.3%
Exp	Poly2	88.6%
Poly2	Exp	87.1%
Poly2	Poly2	86.6%
Exp	Lin	78.5%

SVHN dataset. We now consider the SVHN dataset, which consists of 32x32 images of digits from Google Street View images, 73 257 for training and 26 032 for testing. Due to the larger dataset size, we only consider

⁴Note that in this case the ZCA/whitening step is applied on these larger 6x6 patches.

the kernel approximation approach of Mairal (2016) based on the Nyström method, which projects the patch kernel feature maps at each layer to finite-dimensional subspaces generated by a set of anchor points (playing the role of convolutional filters), themselves computed via a K-means clustering of patches. We train one-versus-all classifiers on the resulting finite-dimensional representations using regularized ERM with the squared hinge loss, and simply report the best test accuracy over a logarithmic grid of choices for the regularization parameter, ignoring model selection issues in order to assess approximation properties. We use the same ZCA preprocessing as on Cifar10 and the same architecture as in Table 1, with a relatively small number of filters (256 at the first layer, 4096 at the second layer, leading to representations of dimension 65 536), noting that the accuracy can further improve when increasing this number. Our observations are similar to those for the Cifar10 dataset: using a degree-3 polynomial kernel at the second layer reaches very similar accuracy to the exponential kernel; using a degree-2 polynomial leads to a slight drop, but a smaller drop than when making this same change at the first layer; using a linear kernel at the second layer leads to a much larger drop. This again highlights the importance of using non-linear kernels on top of the first layer in order to capture interactions at larger scales than the scale of a single patch.

C Extensions to more layers

In this section, we study the RKHS for convolutional kernels with more than 2 convolutional layers, by considering the simple example of a 3-layer convolutional kernel K_3 defined by the feature map

$$\Psi(x) = A_3 M_3 P_3 A_2 M_2 P_2 A_1 M_1 P_1 x,$$

with quadratic kernels at the second and third layer, *i.e.*, $k_2(z, z') = (\langle z, z' \rangle)^2$ and $k_3(z, z') = (\langle z, z' \rangle)^2$. By isomorphism, we may consider the sequence of Hilbert spaces \mathcal{H}_ℓ to be $\mathcal{H}_1 = \mathcal{H}$, $\mathcal{H}_2 = (\mathcal{H} \otimes \mathcal{H})^{|S_2| \times |S_2|}$, and $\mathcal{H}_3 = (\mathcal{H}^{\otimes 4})^{|S_3| \times |S_2| \times |S_2|}$. For some domain Ω , we define the operators $\text{diag}_2 : L^2(\Omega^4) \rightarrow L^2(\Omega^2)$ and its adjoint $\text{diag}_2 : L^2(\Omega^2) \rightarrow L^2(\Omega^4)$ by

$$\begin{aligned} \text{diag}_2(M)[u, v] &= M[u, u, v, v] \quad \text{for } M \in L^2(\Omega^4) \\ \text{diag}_2(M)[u_1, u_2, u_3, u_4] &= \mathbb{1}\{u_1 = u_2\} \mathbb{1}\{u_3 = u_4\} M[u_1, u_3] \quad \text{for } M \in L^2(\Omega^2). \end{aligned}$$

We may then describe the RKHS as follows.

Proposition 3 (RKHS of 3-layer CKN with quadratic $k_{2/3}$). *The RKHS of K_3 when k_2 and k_3 are quadratic kernels $(\langle \cdot, \cdot \rangle)^2$ consists of functions of the form*

$$f(x) = \sum_{\alpha \in (S_3 \times S_2 \times S_2)^2} \sum_{u_1, u_2, u_3, u_4 \in \Omega} G_\alpha[u_1, u_2, u_3, u_4](x_{u_1}, x_{u_2}, x_{u_3}, x_{u_4}), \quad (8)$$

where $G_\alpha \in L^2(\Omega^4, \mathcal{H}^{\otimes 4})$ obeys the constraint

$$G_\alpha \in \text{Range}(E_\alpha), \quad (9)$$

where the linear operator $E_\alpha : L^2(\Omega_3) \rightarrow L^2(\Omega^4)$ for $\alpha = (p, q, r, p', q', r')$ (with $p, p' \in S_3$ and $q, r, q', r' \in S_2$) is defined by

$$E_\alpha x = A_{1,\alpha}^\top \text{diag}_2(A_{2,\alpha}^\top \text{diag}(A_3^\top x)).$$

The operators $A_{1,\alpha}$ and $A_{2,\alpha}$ denote:

$$\begin{aligned} A_{1,\alpha} &= L_q A_1 \otimes L_r A_1 \otimes L_{q'} A_1 \otimes L_{r'} A_1 \\ A_{2,\alpha} &= L_p A_2 \otimes L_{p'} A_2. \end{aligned}$$

The squared RKHS norm $\|f\|_{\mathcal{H}_{K_3}}^2$ is then equal to the minimum over decompositions (8) of the quantity

$$\sum_{\alpha} \|A_3^{-\top} \text{diag}(A_{2,\alpha}^{-\top} \text{diag}_2(A_{1,\alpha}^{-\top} G_\alpha))\|_{L^2(\Omega_3)}^2. \quad (10)$$

The constraint (9) and penalty (10) resemble the corresponding constraint/penalty in the two-layer case for an order-4 polynomial kernel at the second layer, but provide more structure on the interactions, using a multi-scale structure that may model interactions between certain pairs of patches ((x_{u_1}, x_{u_2}) and (x_{u_3}, x_{u_4}) in (8)) more strongly than those between all four patches. In addition to localizing the interactions G_α around certain diagonals, the kernel also promotes spatial regularities: assuming that the spatial bandwidths of A_ℓ increase with ℓ , the functions $(u, v, w_1, w_2) \mapsto G_\alpha[u, u + w_1, u + v, u + v + w_2]$ may vary quickly with w_1 or w_2 (distances between patches in each of the two pairs), but should vary more slowly with v (distance between the two pairs) and even more slowly with u (a global position).

D Proofs

We recall the following result about reproducing kernel Hilbert spaces, which characterizes the RKHS of kernels defined by explicit Hilbert space features maps (see, *e.g.*, Saitoh, 1997, §2.1).

Theorem 4 (RKHS from explicit feature map). *Let H be some Hilbert space, $\psi : \mathcal{X} \rightarrow H$ a feature map, and $K(x, x') = \langle \psi(x), \psi(x') \rangle_H$ a kernel on \mathcal{X} . The RKHS \mathcal{H} of K consists of functions $f = \langle g, \psi(\cdot) \rangle_H$, with norm*

$$\|f\|_{\mathcal{H}} = \inf\{\|g'\|_H : g' \in H \text{ s.t. } f = \langle g', \psi(\cdot) \rangle_H\} \quad (11)$$

D.1 Proof of Proposition 1 (RKHS of One-Layer Convolutional Kernel)

Proof. From Theorem 4, the RKHS contains functions of the form

$$f(x) = \langle F, A\Phi(x) \rangle_{L^2(\Omega_1, \mathcal{H})},$$

with RKHS norm equal to the minimum of $\|F\|_{L^2(\Omega_1, \mathcal{H})}$ over such decompositions.

We may alternatively write $f(x) = \langle G, \Phi(x) \rangle_{L^2(\Omega, \mathcal{H})}$ with $G = A^\top F$. The mapping from F to G is one-to-one if $G \in \text{Range}(A^\top)$. Then, we obtain that equivalently, the RKHS contains functions of this form, with $G \in \text{Range}(A^\top)$, and with RKHS norm equal to the minimum of $\|A^{-\top}G\|_{L^2(\Omega_1, \mathcal{H})}$ over such decompositions. \square

D.2 Proof of Proposition 2 (RKHS of 2-layer CKN with quadratic k_2)

Proof. From Theorem 4, the RKHS contains functions of the form

$$f(x) = \langle F, A_2 M_2 P_2 A_1 \Phi_1(x) \rangle_{L^2(\Omega_2, \mathcal{H}_2)},$$

with RKHS norm equal to the minimum of $\|F\|_{L^2(\Omega_2, \mathcal{H}_2)}$ over such decompositions. Here, $\Phi_1(x) \in L^2(\Omega, \mathcal{H})$ is given by $\Phi_1(x)[u] = \varphi_1(x_u)$, so that $\Phi(x)$ in the statement is given by $\Phi(x) = \Phi_1(x) \otimes \Phi_1(x)$. We also have that $\mathcal{H}_2 = (\mathcal{H} \otimes \mathcal{H})^{|S_2| \times |S_2|}$, so that we may write $F = (F_{pq})_{p, q \in S_2}$ with $F_{pq} \in L^2(\Omega_2, \mathcal{H} \otimes \mathcal{H})$.

For $p, q \in S_2$, denoting by L_c the translation operator $L_c x[u] = x[u - c]$, we have

$$\begin{aligned} (M_2 P_2 A_1 \Phi_1(x)[u])_{pq} &= L_p A_1 \Phi_1(x)[u] \otimes L_q A_1 \Phi_1(x)[u] \\ &= \text{diag}(L_p A_1 \Phi_1(x) \otimes L_q A_1 \Phi_1(x))[u] \\ &= \text{diag}((L_p A_1 \otimes L_q A_1) \Phi(x))[u]. \end{aligned}$$

Then, we have

$$\begin{aligned} \langle F_{pq}, (A_2 M_2 P_2 A_1 \Phi_1(x))_{pq} \rangle_{L^2(\Omega_2, \mathcal{H} \otimes \mathcal{H})} &= \langle F_{pq}, A_2 \text{diag}((L_p A_1 \otimes L_q A_1) \Phi(x)) \rangle_{L^2(\Omega_2, \mathcal{H} \otimes \mathcal{H})} \\ &= \langle A_2^\top F_{pq}, \text{diag}((L_p A_1 \otimes L_q A_1) \Phi(x)) \rangle_{L^2(\Omega_1, \mathcal{H} \otimes \mathcal{H})} \\ &= \langle \text{diag}(A_2^\top F_{pq}), (L_p A_1 \otimes L_q A_1) \Phi(x) \rangle_{L^2(\Omega_1^2, \mathcal{H} \otimes \mathcal{H})} \\ &= \langle (L_p A_1 \otimes L_q A_1)^\top \text{diag}(A_2^\top F_{pq}), \Phi(x) \rangle_{L^2(\Omega^2, \mathcal{H} \otimes \mathcal{H})}. \end{aligned}$$

We may then write this as $\langle G_{pq}, \Phi(x) \rangle_{L^2(\Omega^2, \mathcal{H} \otimes \mathcal{H})}$ with

$$G_{pq} = (L_p A_1 \otimes L_q A_1)^\top \text{diag}(A_2^\top F_{pq}),$$

and the mapping between $F_{pq} \in L^2(\Omega_2, \mathcal{H} \otimes \mathcal{H})$ and $G_{pq} \in L^2(\Omega^2, \mathcal{H} \otimes \mathcal{H})$ is one-to-one if $G_{pq} \in \text{Range}((L_p A_1 \otimes L_q A_1)^\top)$, and $\text{diag}((L_p A_1 \otimes L_q A_1)^{-\top} G_{pq}) \in \text{Range}(A_2^\top)$. We may then equivalently write the RKHS norm as the minimum over G_{pq} satisfying such constraints for all $p, q \in S_2$, of the quantity

$$\sum_{p, q \in S_2} \|F_{pq}\|^2 = \sum_{p, q \in S_2} \|A_2^{-\top} \text{diag}((L_p A_1 \otimes L_q A_1)^{-\top} G_{pq})\|_{L^2(\Omega_2, \mathcal{H} \otimes \mathcal{H})}^2.$$

□

D.3 Proof of Proposition 3 (RKHS of 3-layer CKN with quadratic $k_{2/3}$)

Proof. Let $\Phi(x) = (\varphi_1(x_u))_u \in L^2(\Omega, \mathcal{H})$, so that we may write

$$\sum_{u_1, u_2, u_3, u_4 \in \Omega} G[u_1, u_2, u_3, u_4](x_{u_1}, x_{u_2}, x_{u_3}, x_{u_4}) = \langle G, \Phi(x)^{\otimes 4} \rangle_{L^2(\Omega^4, \mathcal{H}^{\otimes 4})},$$

for some $G \in L^2(\Omega^4, \mathcal{H}^{\otimes 4})$.

From Theorem 4, the RKHS contains functions of the form

$$f(x) = \langle F, A_3 M_3 P_3 A_2 \Phi_2(x) \rangle_{L^2(\Omega_3, \mathcal{H}_3)}, \quad (12)$$

with RKHS norm equal to the minimum of $\|F\|_{L^2(\Omega_3, \mathcal{H}_3)}$ over such decompositions. Here, $\Phi_2(x) \in L^2(\Omega_1, \mathcal{H}_2) = L^2(\Omega_1, (\mathcal{H} \otimes \mathcal{H})^{|S_2| \times |S_2|})$ is given as in the proof of Proposition 2, by

$$\Phi_{2,qr}(x)[u] = \text{diag}((L_q A_1 \otimes L_r A_1)(\Phi(x) \otimes \Phi(x)))[u],$$

for $q, r \in S_2$. A patch $P_3 A_2 \Phi_2(x)[u]$ is then given by

$$P_3 A_2 \Phi_2(x)[u] = (L_p A_2 \Phi_{2,qr}(x)[u])_{p \in S_3, q, r \in S_2} \in (\mathcal{H} \otimes \mathcal{H})^{|S_3| \times |S_2| \times |S_2|}.$$

Applying the quadratic feature map given by $\varphi_3(z) = z \otimes z \in (\mathcal{H}^{\otimes 4})^{(|S_3| \times |S_2| \times |S_2|)^2}$ for $z \in (\mathcal{H} \otimes \mathcal{H})^{|S_3| \times |S_2| \times |S_2|}$, we obtain for $\alpha = (p, q, r, p', q', r') \in (S_3 \times S_2 \times S_2)^2$,

$$\begin{aligned} (M_3 P_3 A_2 \Phi_2(x)[u])_\alpha &= L_p A_2 \Phi_{2,qr}(x)[u] \otimes L_{p'} A_2 \Phi_{2,q'r'}(x)[u] \\ &= \text{diag}(A_{2,\alpha}(\Phi_{2,qr}(x) \otimes \Phi_{2,q'r'}(x)))[u], \end{aligned}$$

where

$$A_{2,\alpha} = L_p A_2 \otimes L_{p'} A_2.$$

Now, one can check that we have the following relation:

$$\begin{aligned} \Phi_{2,qr}(x) \otimes \Phi_{2,q'r'}(x) &= \text{diag}((L_q A_1 \otimes L_r A_1)(\Phi(x) \otimes \Phi(x))) \otimes \text{diag}((L_{q'} A_1 \otimes L_{r'} A_1)(\Phi(x) \otimes \Phi(x))) \\ &= \text{diag}_2(A_{1,\alpha} \Phi(x)^{\otimes 4}), \end{aligned}$$

with

$$A_{1,\alpha} = L_q A_1 \otimes L_r A_1 \otimes L_{q'} A_1 \otimes L_{r'} A_1.$$

Since $\mathcal{H}_3 = (\mathcal{H}^{\otimes 4})^{(|S_3| \times |S_2| \times |S_2|)^2}$, we may write $F = (F_\alpha)_{\alpha \in (S_3 \times S_2 \times S_2)^2}$, with each $F_\alpha \in L^2(\Omega_3, \mathcal{H}^{\otimes 4})$. We then have

$$\begin{aligned} \langle F_\alpha, (A_3 M_3 P_3 A_2 \Phi_2(x))_\alpha \rangle_{L^2(\Omega_3)} \\ &= \langle F_\alpha, A_3 \text{diag}(A_{2,\alpha} \text{diag}_2(A_{1,\alpha} \Phi(x)^{\otimes 4})) \rangle_{L^2(\Omega_3)} \\ &= \langle \text{diag}(A_3^\top F_\alpha), A_{2,\alpha} \text{diag}_2(A_{1,\alpha} \Phi(x)^{\otimes 4}) \rangle_{L^2(\Omega_2^2)} \\ &= \langle \text{diag}_2(A_{2,\alpha}^\top \text{diag}(A_3^\top F_\alpha)), A_{1,\alpha} \Phi(x)^{\otimes 4} \rangle_{L^2(\Omega_1^4)} \\ &= \langle A_{1,\alpha}^\top \text{diag}_2(A_{2,\alpha}^\top \text{diag}(A_3^\top F_\alpha)), \Phi(x)^{\otimes 4} \rangle_{L^2(\Omega^4)}. \end{aligned}$$

We may write this as $\langle G_\alpha, \Phi(x)^{\otimes 4} \rangle_{L^2(\Omega^4, \mathcal{H}^{\otimes 4})}$, with

$$G_\alpha = A_{1,\alpha}^\top \operatorname{diag}_2(A_{2,\alpha}^\top \operatorname{diag}(A_3^\top F_\alpha)).$$

The mapping from F_α to G_α is bijective if G_α is constrained to the lie in the range of the operator E_α . If G_α satisfies this constraint, we may write

$$F_\alpha = A_3^{-\top} \operatorname{diag}(A_{2,\alpha}^{-\top} \operatorname{diag}_2(A_{1,\alpha}^{-\top} G_\alpha)).$$

Then, the resulting penalty on G_α is as desired. □